European Journal of Business & Social Sciences
Available at https://ejbss.org/
ISSN: 2235-767X
Volume 07 Issue 01
January 2019

Photothermal Analysis of Buffer Layer Material and Thin Film Solar Cells

Shamim Akhtar [1], Dr. Mohan Nathulal Giriya

[1]Research Scholar, Department of Physics, Sri Satya Sai University of Technology & Medical Sciences, Sehore, MP(India)

ABSTRACT

This study deals with analysis of In2S3 thin films, which are used as buffer layer material in solar cells. The various influences of film composition, chlorine and silver incorporation in this material is brought out from the measurement of transport properties and analysis of sub band gap levels. The application of photothermal deflection technique for characterization of solar cells is a relatively new area that requires considerable attention. Thus, elucidates the theoretical aspects of application of photothermal techniques for solar cell analysis. The experimental design and method for determination of solar cell efficiency, optimum load resistance and series resistance with results from the analysis of CuInS2/In2S3 based solar cell.

KEYWORDS : Photothermal, thin film, buffer layer, solar cell

1.0 INTRODUCTION

Optimization of junction layers of a solar cell is essential for achieving its high performance. In thin film solar cells, buffer layers are used to enhance empirical V_{OC} and this effectively improves the junction efficiency [1]. Buffer layer, when used near the top of a cell, is beneficial for optical enhancement because of reduced absorption and reflection losses. This layer in a solar cell is also responsible for a number of effects that significantly influence the efficiency of solar cells [2]. For example, it assists in improving the cells efficiency by separating the contact, which has high minority-carrier recombination loss from the absorber or base layer. An effective injection of carriers (between the face electrode and the absorbing layer) and a maximum transmission of light can be attained by using optimum material as the buffer layer. This layer is usually made from high-optical-quality, *n*-type films based on a wide band gap semiconductor compound. A wide band-gap material is well suited for efficiently transmitting the blue spectrum of sunlight to the PN junction, thus enhancing the solar cell efficiency. One of the most promising buffer materials suitable for this purpose is In_2S_3. It is a wide band gap material (2.6 eV) [3] and cells, fabricated using In_2S_3 as the buffer layer, have shown efficiency as high as 16.4%[4]. This material has been widely used to replace the use of toxic CdS layer [5]. Materials such as ZnO, ZnSe, $ZnIn_xSe_y$ and In_xSe_y are also promising candidates to be used as buffer materials in CIS based solar cells.

Motivation for the present work on photothermal analysis of In_2S_3 films is the earlier studies done on spray pyrolysed In_2S_3 films by our group. These works have revealed several

interesting aspects of the material and could also produce cells with high efficiency [6]. We studied how the film composition and dopant affect the non-radiative transitions and transport properties of the material; these results were applied for improving the fabrication process to achieve better transport properties and to produce more effective solar cell junction.

Indium sulphide

In_2S_3 belonging to III-VI group is a wide band gap semiconductor with high absorption coefficient and intense luminescence [7] and is a promising buffer layer material for compound semiconductor heterojunction thin film solar cell. It crystallizes in spinel structure and exists in four crystallographic modifications. Room temperature phase of β-In_2S_3 crystallizes in defect spinel structure with high degree of vacancies in tetrahedral sites [8]. There are several works reporting the electrical and optical characterization and tuning of the properties of β- In_2S_3 films [14, 15, 16]. In_2S_3 buffer layers deposited using the 'Spray-Ion Layer Gas Reaction (Spray-ILGAR)' technique have recently been used with Cu (In, Ga)(S, Se) $_2$ as absorber, resulting in cells with an efficiency of 13.1% which is equal to that obtained from CdS based cells [19]. It is thus viewed as a potential eco-friendly material replacing toxic cadmium in CIGS based solar cells [20]. Spiering et al deposited In_2S_3 buffer layer employing MOVCD with Cu (In, Ga) Se_2 as absorber and reported an efficiency of 12.3% [21]. Teny et al fabricated $CuInS_2/In_2S_3$ solar cells with 9.5 % efficiency using CSP technique [6].

The interesting optical and electrical properties exhibited by this material motivated the present work on photothermal analysis of In_2S_3 films. β-In_2S_3 films are inherently n-type and the grains showed preferential orientation along 220 planes. Depending on the film composition, band gap was reported to vary from 2.64 eV to 2.71 eV and these films had high absorption coefficient of order 10^5 cm^{-1} in blue region. The aim is to study how the defects contribute to non-radiative nature and transport properties of the film.

1.1 FABRICATION OF INDIUM SULPHIDE THIN FILMS

β-In_2S_3 thin films were deposited over glass slides (37 × 12 × 1.4 Mm^3) using CSP technique [13]. The films were fabricated with indium chloride and thiourea as precursor solution, keeping the spray volume at 400 ml, spray rate at 20 ml/min and substrate temperature at 300^0C. Stoichiometry of the films was varied by adjusting the molarity of the precursor solutions. Films chosen for the photothermal analysis had different compositions with In/S as 0.64, 0.68 and 0.79 (coded as, P_1, P_2, and P_3 respectively). All these films (P-series), which had indium chloride as a precursor, contained traces of chlorine existing as an inherent dopant [13]. To obtain films with no chlorine, another set of films (coded D-series), were fabricated under similar deposition conditions using indium nitrate and thiourea as precursors. Chlorine was subsequently introduced in to the samples, in calculated amount, by adding ammonium chloride in the spray solution. The amount of chlorine incorporated in the film was controlled by varying the quantity of ammonium chloride (3.5 ml, 5.5 ml, 7.5 ml). These samples, in which chlorine was deliberately incorporated, were coded as D_1, D_2

European Journal of Business & Social Sciences
Available at https://ejbss.org/
ISSN: 2235-767X
Volume 07 Issue 01
January 2019

and D_3 respectively and the film with no chlorine was coded as D_0.

1.2 PHOTOTHERMAL ANALYSIS OF β-INDIUM SULPHIDE THIN FILMS

Samples of size 1×1 cm^2 were irradiated using CW laser beams of 'above band gap' energy (2.81 eV) and 'sub band gap' (2.33 eV and 1.96 eV) with power 10 mW to analyse their photothermal response. The power of all three incident beams was maintained at 10 mW using ND filters. In β-In_2S_3 films, irradiated with beam of energy 2.81 eV, carriers are excited from valence band to highest possible level of conduction band. Later they de-excite by thermal emission to the minimum of conduction band (intra band transitions) and some diffuse before they recombine; other carriers recombine radiatively or non-radiatively and relax back to valence band. Thermal waves thus generated produce photothermal signals whose signal amplitude varies with chopping frequency.

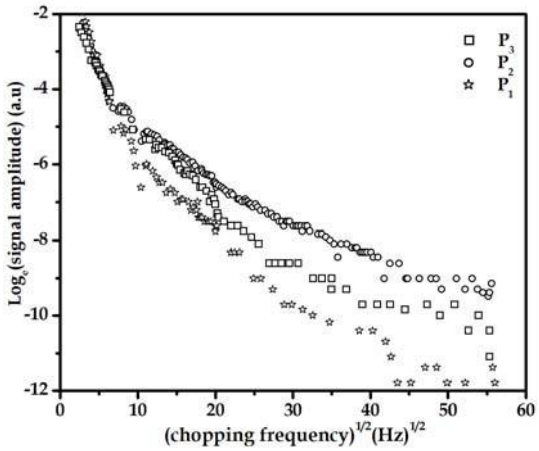

Figure 1.1 PTBD response of samples P_1, P_2 and P_3 upon 2.81 eV excitation

Variation of slope of the photothermal signal with chopper frequency in the lower frequency is an indication of the intraband transitions occurring in the material and response in higher frequency region implies the presence of non-radiative recombination centres in the bulk and surface of the material. Photothermal responses of samples P_1, P_2 and P_3 are depicted in figure 1.1.

The signals due to intra-band transitions are almost the same in all the three samples and as the frequency reaches 100 Hz, the response is lowest for P_1 having least In/S (0.64) and highest for sample P_2 (In/S 0.68). But for sample P_3 with highest In/S (.79) the non- radiative emission is lower than P_2. Hence the defect density is higher for sample P_2. Table 1.1 shows the EDAX measurements of samples P_1, P_2 and P_3.

European Journal of Business & Social Sciences
Available at https://ejbss.org/
ISSN: 2235-767X
Volume 07 Issue 01
January 2019

Table 1.1 :EDAX report of the β-In_2S_3 films with 'inherent' chlorine (P series)

Sample Code	Is/S	Cl	Cl/In+S
P_1	0.64	8.6	0.094
P_2	0.68	10.77	0.12
P_3	0.79	15.38	0.18

Table 1.2 : Transport properties of P-series sample

Sample Code	$D_s(10^{-4}m^2/s)$	μ (cm^2/Vs)	$V_{sr}\times10^3$ (cm/s)	τ_r (μs)
P_1	9	0.46	5	100
P_2	8.4	2.0	10	100
P_3	10	2.68	5	100

Table 1.2 shows the transport properties obtained using PTBD technique. V_{sr} was highest ($1x10^4$cm/s) for P_2, while it was almost same for other samples. High V_{sr} indicates the presence of more surface defects in film P_2, which contribute to the high non-radiative losses. However emained same (100 μs) for all samples. μ was high for P_2 and P_3 with values 2.68 and 2.0 cm^2/V_s respectively. Higher non-radiative loss is an indication of high defect density and there is a tendency to affect the transport properties by shortening the carrier diffusion length due to scattering and / or recombination of carriers at defects. But in this case, we find mobility is high for samples (P_1 and P_2), which showed high PTBD signal. Variation in V_{sr} alone with no change in lifetime in the sample suggests that bulk defects are not very much affected with change in composition. Hence for films with high chlorine incorporation, scattering of carriers at grain boundaries is reduced considerably and this increased the carrier mobility.

European Journal of Business & Social Sciences
Available at https://ejbss.org/
ISSN: 2235-767X
Volume 07 Issue 01
January 2019

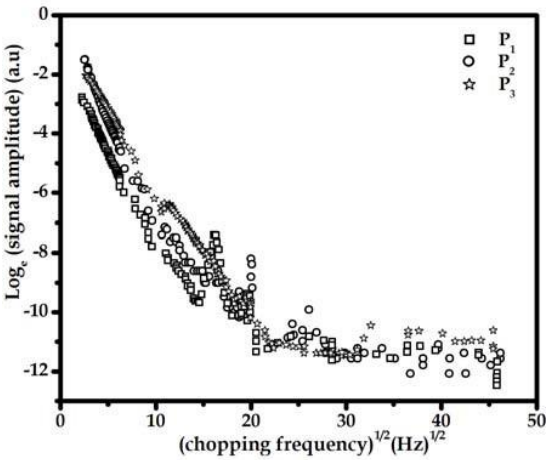

Figure 1.2a PTBD signal response on excitation using 2.33 eV

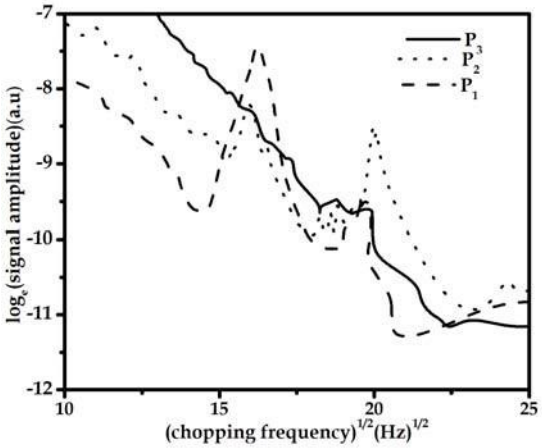

Figure 1.2b PTBD signal response in 100 Hz to 500 Hz for P_1, P_2, P_3 upon 2.33 eV excitation

All the facts suggest that incorporation of chlorine has major role in altering the transport properties of the In_2S_3 films. To study the role of chlorine in creation of defect levels that can cause non-radiative losses, the films were excited using 2.33 eV and 1.96 eV. Upon excitation using 2.33 eV, the carriers were possibly excited from the valence band to a defect level formed due to vacancy of sulphur (V_S). Hence the photothermal response we observe here is due to the relaxation of carriers from this defect level. Figure 1.2a and 1.2b show the photothermal signal plot of samples P_1, P_2 and P_3 when excited using 2.33 eV. The photothermal response due to 2.33 eV is highest for P_3 and decreases for P_2 and P_1 with the decrease in In/S ratio. The samples P_1 and P_2 show a peak at high frequency (> 200 Hz), with the peak intensity being higher for sample P_1 while for sample P_3 this peak is not seen (figure 1.2b). Such peaks are due to the non-radiative emission occurring at the non-radiative recombination centres. The photothermal response obtained on excitation using 1.96 eV carriers were due to deexcitation from conduction band because the absorption of 1.96 eV can excite the carriers from defect level O_{VS} to conduction band (Figure 1.2b). Figure 1.3

European Journal of Business & Social Sciences
Available at https://ejbss.org/
ISSN: 2235-767X
Volume 07 Issue 01
January 2019

illustrates the photothermal signal variation of P_1, P_2 and P_3 with 1.96 eV, where we find the non-radiative emission varies only slightly with signal; this is the highest for P_2, similar to the result due to excitation using 2.81 eV. For understanding the photothermal response of each sample at different excitation wavelength and hence realise the role of defects in affecting the signal response due to sub band gap energy absorption, we plotted the photothermal response for 2.81 eV, 2.33 eV and 1.96 eV (Figure 5.6 a, 5.6 b and 5.6 c for samples P_1, P_2 and P_3 respectively).

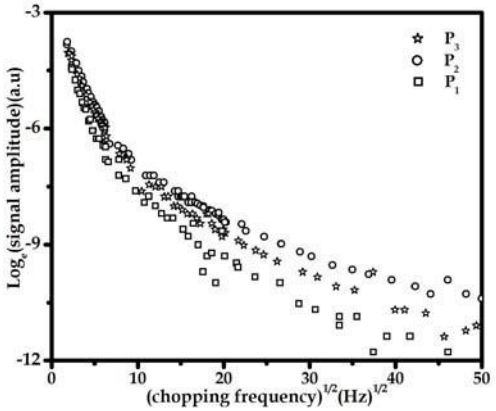

Figure 1.3 PTBD signal response of P_1, P_2 and P_3 due to 1.96 eV excitation

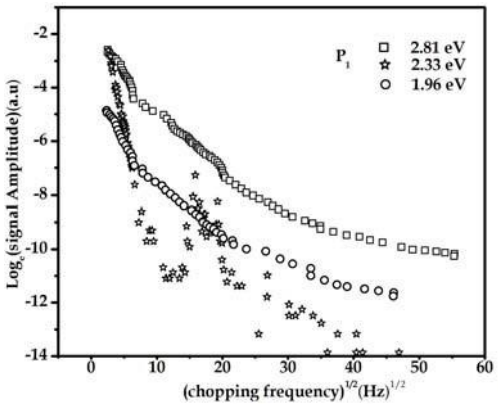

Figure 1.4a Photothermal responses of P_1 on excitation with 2.81, 2.33, 1.96 eV

European Journal of Business & Social Sciences
Available at https://ejbss.org/
ISSN: 2235-767X
Volume 07 Issue 01
January 2019

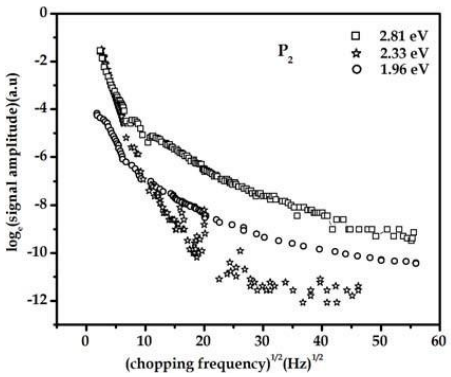

Figure 1.4b Photothermal response of P_2 on excitation with 2.81, 2.33, 1.96 eV

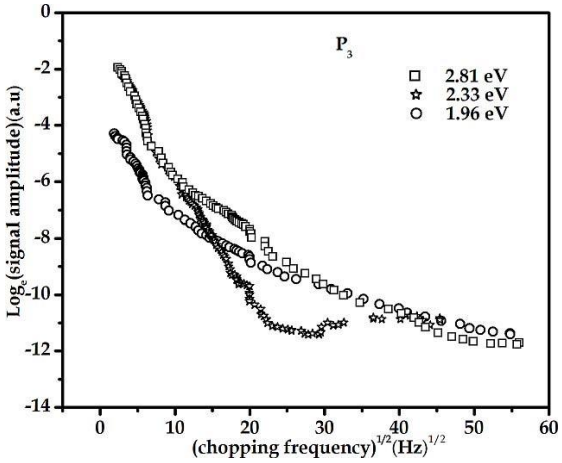

Figure 1.4c Photothermal response of samples 2.33 eV

For sample P_1 (Figure 1.4a), the slope of photothermal signal variation for 2.33 eV excitation shows a rapid decline (in frequency regime < 200 Hz), whereas the slope of the signal for both 2.81 eV and 1.96 eV excitation varies slowly. The signal variation for chopping frequency < 200 Hz is due to intra-band transitions. For the 'above-band gap' excitations, (i.e., using 2.81 eV), the photothermal signal is due to transitions occurring within the conduction band and hence these signals are strong and their decrease with chopping frequency is rather slow. But for 2.33 eV excitation, the carriers can reach only the defect level due to V_S and interestingly this defect level is appearing to be a 'defect band' [24]. The photothermal signal due to transition of carriers from V_S is naturally weak as there is low number of carriers in the defect band and hence decreases rapidly i.e., the level V_S is localized and less dense in sample P_1. But for sample P_2 (Figure 1.4b) the photothermal signal due to 2.33 eV excitation is stronger (higher amplitude) in low frequency regime and signal variation is more gradual than sample P_1. This indicates that the 'defect band' V_S is denser and hence the probability of non-radiative (intraband) transitions occurring in this level is also higher in this sample. For sample P_3 (Figure 1.4c), the photothermal response due to 2.33 eV excitation (frequency region < 200 Hz) is same as the signal variations due to

European Journal of Business & Social Sciences
Available at https://ejbss.org/
ISSN: 2235-767X
Volume 07 Issue 01
January 2019

2.81 eV. This implies that the defect Vs is much denser and appears as a wider 'defect band'. So for sample P_3, the signal due to non-radiative transitions occurring in the defect band is similar to that due to transitions occurring in the conduction band. We may conclude that for sample P_3 for which In: S is least and Cl content is high, the defect V_S exist as a band and for sample P_1 for which the In: S is high and Cl content is low the defect V_S is localized.

The amplitude of photothermal signal due to irradiation with 1.96 eV is lower while nature of the signal variation is similar to that due to 2.81 eV excitation for all the samples (Figure a, b and c). This indicates that the signal due to 1.96 eV excitation is resulting from transitions occurring within the conduction band. Thus, from photothermal analysis we can also understand the nature of the defect in which the non-radiative transitions take place.

The transport parameters μ and V_{sr} calculated from the photothermal signal due to absorption of 1.96 eV are almost of same order as that for 2.81 eV. But for 1.96 eV excitation τ_r is slightly higher (150 μs); this could be due to the lower number of carrier available in conduction band. As a result, the carrier scattering is reduced when excitation is from a defect level to conduction band rather than from valence band and hence the carriers can propagate farther before they recombine. However the transport properties measured from the signal obtained for 2.33 eV (Table 1.3) are higher than that obtained for 2.81 eV (Table 1.2). The mobility in the defect level is highest for P_3 where the defect level exists as a band. The mobility in extended states is higher than that for localized defect states as the motion of carriers occur by hopping conduction, which is a thermally activated tunnelling between states.

Table 1.3 : Transport properties of P_1, P_2, and P_3 (excitation using 2.33 eV)

Sample	D_s ($10^{-4}cm^2/s$)	μ (cm^2/Vs)	V_{sr} (cm/s)	τ (μs)
P_1	7.4	1.6	5×10^5	0.1
P_2	8.7	9.63	2×10^5	0.1
P_3	9.3	7.4	2×10^5	0.1

Table 1.4 : EDAX report of the β-In_2S_3 films with 'doped' chlorine (D series)

Sample Code	In/S	Cl	Cl/In+S
D_0	0.65	0	0
D_1	0.70	3	0.03
D_2	0.74	10.58	0.12
D_3	0.75	12.5	0.14

Mobility was highest for sample P_3, which had high In/S and high chlorine incorporation. To deduce the role of chlorine in improving the transport properties and deciding the defect

European Journal of Business & Social Sciences
Available at https://ejbss.org/
ISSN: 2235-767X
Volume 07 Issue 01
January 2019

nature of the film, we performed PTBD analysis on films with no chlorine D_0 and those containing chlorine in increasing amount ie. Samples D_1, D_2 and D_3 respectively. The atomic concentration of In: S and Cl incorporated in the film is shown in table 1.4. Figure shows the plot of (modulation frequency)$^{1/2}$ versus Log$_e$ (signal amplitude) for samples D_0, D_1, D_2, D_3 when excited using 2.81 eV. The photothermal signal is slightly higher for sample D_0 than the other chlorine incorporated films. The density of defects, leading to non-radiative heat losses, is higher in chlorine free films and decreases with increase in chlorine incorporation. The transport parameters D_s, V_{sr}, μ and τ_r obtained for D series samples are shown in Table 1.4. We find that μ is highest for D_3 films in which chlorine incorporation is higher. The V_{sr} is lowest (7 $\times 10^3$ cm/s) and τ_r is highest (130 μs) for D_2 which has considerably high Cl content compared to D_1. Mobility and lifetime are the least for D_0 films, which contains no trace of chlorine. Therefore incorporation of chlorine certainly plays an active role in improving the transport properties by controlling the density of V_S and V_{In} in the film.

Figure 1.5 Photothermal signal responses of samples D_0, D_1, D_2, D_3 on 2. 81 eV excitation

Table 1.5 : Transport properties of D-series sample

Sample	D_s (10^{-4}cm^2/s)	μ (cm^2/Vs)	V_{sr} (cm/s)	τ (μs)
D_0	9.2	0.23	11	30
D_1	9	0.38	11	90
D_2	9.2	0.48	7	130
D_3	8	0.60	11	50

Upon excitation with 2.33 eV, the photothermal response, which occurs due to transitions in defect band V_S, was highest for samples with high chlorine incorporation D_3, thus indicating that chlorine incorporation assist in creation of V_S and thus enhancing the absorption of 2.33 eV (Figure 1.5). In EDAX report (Table 1.5) also we find that sulphur content decreases with increase in chlorine, leading to high V_S density.

European Journal of Business & Social Sciences
Available at https://ejbss.org/
ISSN: 2235-767X
Volume 07 Issue 01
January 2019

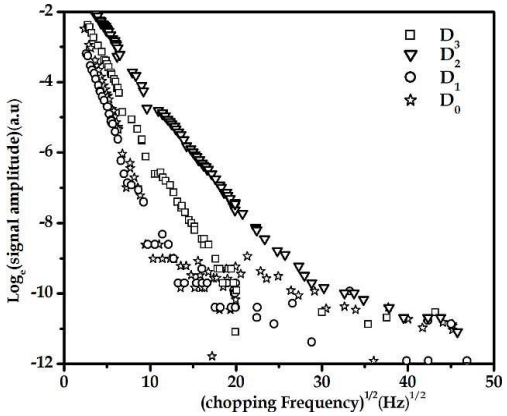

Figure 1.6 : Photothermal signal response of samples D_0, D_1, D_2, D_3 on 2.33 eV excitation

In figure 1.6, showing the PT response for D_0, we find that PTBD signal variation for 2.33 eV is unlike the signal obtained for 2.81 eV. In this sample, the thermal contribution due to intra-band transition within defect band V_S is very low and the small peak that is seen at frequency > 300 Hz is due to non-radiative recombinations alone, where as in D_3 and D_2, the defect band due to V_S is well formed and thermal emission from intra-band transition and non-radiative recombination equally contribute to the PTBD signal generation. For these samples at lower frequency < 300 Hz, the signal amplitude is similar to that on excitation with 2.81 eV. In figure 1.7b for sample D_2, we observe that PT signal variation due to 2.33 eV excitation is almost similar to that for 2.81 eV. These results are similar to those obtained for P-series sample where we were quite uncertain about the role of chlorine due to the variation in In/S during fabrication. These results confirm that chlorine is responsible for non-radiative transitions occurring in the defect level that causes absorption of 2.33 eV, as the In/S constituents were kept constant during fabrication and only the chlorine content was varied. But on excitation with 1.96 eV, only sample D_3 showed PT response (Figure 1.8). The absorption of 1.96 eV is considered to be due to excitation of carriers from OV_S to conduction band. So, in the D-series samples, OV_S defects are lower and oxygen incorporation in sulphur vacancy is reduced.

Photothermal analysis of β-In_2S_3 films upon excitation using 2.81 eV, 2.33 eV and 1.96 eV impart better understanding of the non-radiative nature of the film, its dependence on films composition and the influence of chlorine. Sample with highest chlorine showed high mobility. From the analysis of samples, which contain accidental incorporation of chlorine (P series) and calculated quantity of chlorine (D series), we could prove that incorporation of chlorine improves the absorption of 2.33 eV due to creation of defect band V_S. PTBD technique is thus demonstrated as an efficient tool for defect analysis of semiconductors.

European Journal of Business & Social Sciences
Available at https://ejbss.org/
ISSN: 2235-767X
Volume 07 Issue 01
January 2019

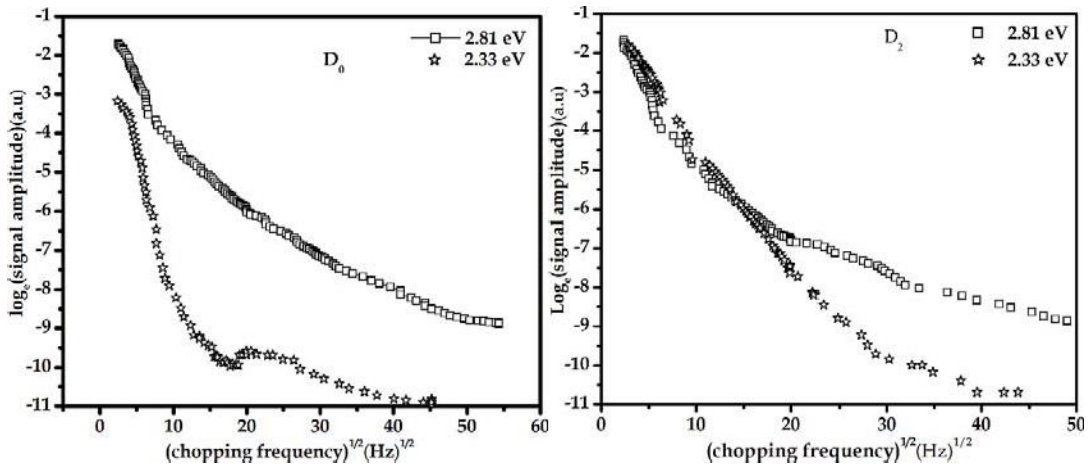

(a) (b)

Figure 1.7 : Photothermal response for 2.81 eV and 2. 33 eV excitation of samples (a) D_0 and (b) D_2

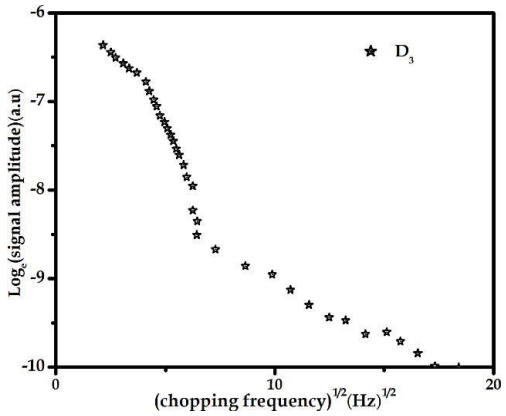

Figure 1.8 Photothermal response of samples D_3 on 1.96 eV excitation

Fabrication

Films were deposited with $InCl_3$ and thiourea as precursor solution and the composition (In/S) of the film was varied from 1.2/8, 2/8, 2.2/8, 2.5/8, 2.8/8 and 3/8. The spray parameters were the volume of spray solution (200 ml), spray rate (6 ml/min) and substrate temperature (300°C). The other essential details of film fabrication the automated spray unit have described in previous chapter.

Photothermal analysis

The films were irradiated with beams of energy 2.81 eV, 2.33 eV and 1.96 eV. Photothermal

European Journal of Business & Social Sciences
Available at https://ejbss.org/
ISSN: 2235-767X
Volume 07 Issue 01
January 2019

signal is least for the sample 2/8 for "above band gap" excitation (Figure 1.9a), thereby making the non-radiative losses the least for particular composition. But for sub band gap excitations, these films show high photothermal signal (Figure 1.9b and 1.9c), which is also an indication of the absorption-taking place at a defect band in the forbidden gap region.

The transport properties measured are shown in table 1.9. We obtained a high mobility of 30 cm^2/Vs for films prepared at 2/8. But lifetime was highest for 2.5/8 in which the non-radiatve loss is lower. Again lifetime was highest for 2.5/8 (1 ms). On correlating this results with V_{oc} and J_{sc} of $CuInS_2$ based cells fabricated using In_2S_3 as buffer layer, we find that In_2S_3 layer with In/S ratio 2/8 (which offered high mobility and least V_{sr}) showed highest J_{sc} (3.48 mA/cm^2) and cells fabricated with 2.5/8 having high life time gave maximum V_{oc} (306 mV). Figure 1.9 shows the dependence of cells V_{oc} on the lifetime of the buffer layer.

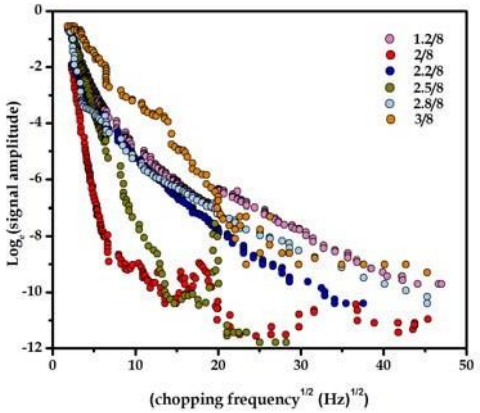

Figure 1.9a Photothermal signal responses for automated spray samples on 2.81 eV

Table 1.6 : Transport properties of buffer layer

Sample	D_s ($\times 10^{-3}$ cm^2/s)	V_{sr} cm^2/s	τr (μs)	μ (cm^2/Vs)
12:8	1.2	2×10^8	200	1.46
2:8	0.8	1×10^7	300	30
2:2:8	0.8	1×10^8	40	0.27
2:5:8	0.8	2×10^7	1000	0.5
2:8:8	0.8	6×10^8	60	3.6
3:8	1.1	1×10^8	500	1.9

European Journal of Business & Social Sciences
Available at https://ejbss.org/
ISSN: 2235-767X
Volume 07 Issue 01
January 2019

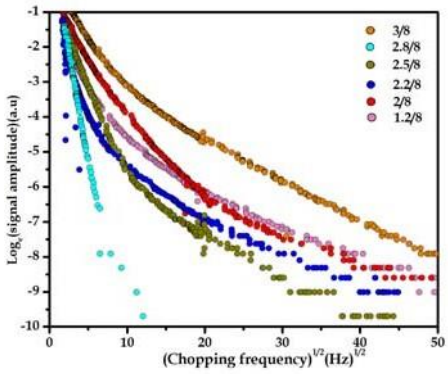

Figure 1.9 b Photothermal signal responses for automated spray samples 2.33 eV

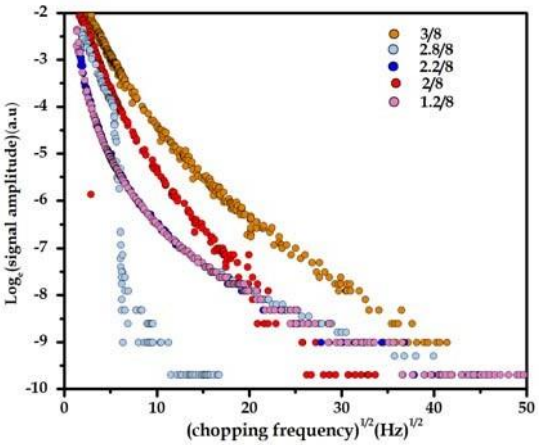

Figure 1.9 c Photothermal signal responses for automated spray samples 1.96 eV

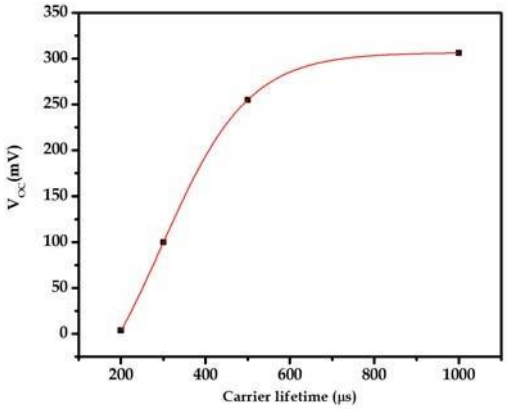

Figure 1.10 Dependence of Voc on carrier lifetime

Ag doped In_2S_3 thin films

Several materials (like Copper, Indium, Aluminium and Silver) are suitable for doping in In_2S_3. But it was silver that offered considerably high J_{sc} and V_{oc}. So to analyse the role of

European Journal of Business & Social Sciences
Available at https://ejbss.org/
ISSN: 2235-767X
Volume 07 Issue 01
January 2019

Ag in optical, electrical, structural properties, studies were carried out on this material that were doped with Ag. Photosensitivity of the films increased from 450 to 538 on Ag doping. Apart from that, resistivity of the films also reduced from $1.2x10^3$ Ω cm to 0.06 Ω cm. The crystallinity of the films improved very much; the grain size increased from 16 nm to 36 nm [29]. Probably because of all these factors, films with Ag electrode produced high efficiency [30].

Fabrication

In_2S_3 films of thickness 0.75 µm were deposited on glass slides using automated chemical spray pyrolysis, with spray rate 8 ml/min, spray volume 200 ml and substrate temperature 300°C and In/S ratio 2/8. On the surface of this film, 13 mg of silver was deposited using vacuum evaporation at 10-6 mbar. We fabricated 3 films; 1) the pure In_2S_3 film were coded as "InS"; 2) In_2S_3 film doped with Ag coded "InS: Ag" and 3) In_2S_3 film doped with Ag and vacuum annealed at 100 0C for one hour under pressure of 10-6 m bar was coded In_2S_3: Ag (100°C).

Photothermal analysis of Ag doped In_2S_3 thin films

Photothermal analysis was done on the films InS, InS: Ag and InS: Ag (100°C) to understand the influence of Ag "doping" and "diffusion" on the materials transport properties. Results of Transport properties obtained using this technique is shown in table 1.7. It is clear that Ag doping has improved the transport properties considerably. For example, the mobility has shot up by ~ 3 times and lifetime increased from 500 µs to 900 µs. Doping of silver has not however helped in reducing the surface defects. In fact the surface recombination increased slightly with doping of Ag. Annealing of Ag enhances the diffusion of Ag into the bulk of the material. Figure 1.11, shows the plot of 'phase' versus 'chopping frequency' for the three films. Photothermal signal phase shows a sudden (step- like) increase when there are 2 layers of different materials due to the difference in thermal diffusivity of the two materials. Such a step change is clear for In_2S_3: Ag. But on annealing this material at 100°C for one hour the dopant diffused into the material and the step change in photothermal signal phase disappeared. But the diffusion of Ag did not improve the transport properties, except that there is a slight decrease in mobility to 0.63 Cm^2/Vs.

Another interesting result of the study is that the Ag deposited on the material surface diffuses into the bulk of the material with time. Figure 1.12 depicts this result; the In_2S_3: Ag existed as 2 different layers till the third day after fabrication. Further analysis and studies are required for finding the depth of diffusion and extracting the information on material properties from different layers.

European Journal of Business & Social Sciences
Available at https://ejbss.org/
ISSN: 2235-767X
Volume 07 Issue 01
January 2019

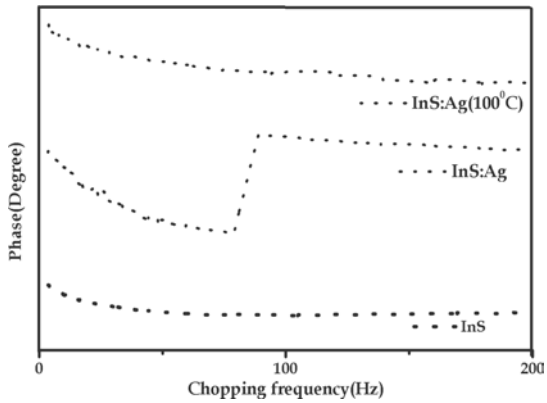

Figure 1.11 Photothermal signal plot versus chopping frequency of Ins, InS: Ag, InS: Ag (100°C)

Table 1.7 : Transport properties of In_2S_3 with and without Ag doping

Sample	D_s ($\times 10^{-3}$ cm^2/s)	V_{sr} cm^2/s	τr (μs)	μ (cm^2/Vs)
InS	0.91	0.27	500	1
InS : Ag	1.1	0.76	900	2
Ins : Ag (100°C)	1.4	0.63	900	2.1

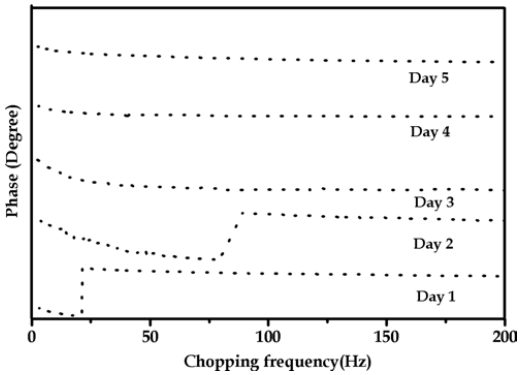

Figure 1.12 : Photothermal signal plot versus chopping of InS: Ag with time (in days)

We explored another interesting application of photothermal deflection technique apart from determining the transport properties of Ag doped In_2S_3 films. Here we have shown that the technique can be used for depth profiling of a film to differentiate the formation of different layers. Ag doping has definitely improved the transport properties of In_2S_3 thin films by increasing the mobility and carrier lifetime.

1.3 PROSPECT OF PT TECHNIQUES FOR SOLAR CELL ANALYSIS

Basic principle of PT and PA techniques is the detection of heat produced in a sample due to

non-radiative de-excitation process, resulting from the absorption of modulated light. Consequently, their signals are proportional to the conversion efficiency of light into heat and, therefore, complementary to the other photo-induced energy conversion processes. This aspect was explored by several research groups for investigating the photo-induced conversion processes ranging from study of photosynthetic processes in leaves to monitoring of photovoltaic conversion efficiency of solar cells and for the study of non-radiative recombination processes in semiconductors [6]. In case of photo-thermal characterization of solar cells, first work was reported in the field using photo-acoustic spectroscopy. Though a variety of photo-thermal spectroscopy techniques were successfully developed, only few of these techniques were found to be useful for photovoltaic cell characterization. These include photo-thermal radiometry, photopyroelectric detection and photo-thermal beam deflection schemes.

The basic phenomenon of direct solar energy conversion into electrical energy involves absorption, and emission of radiation, which are irreversible processes. Consequently, a part of the incoming solar radiation flux is always dissipated as heat within the absorber. In case of solar cells that use unconcentrated radiation, the quantity of dissipated heat can exceed 70% of the incoming energy flux. Usually this heat is lost to the ambient. But this mechanism of heat rejection is rarely considered in the literature i.e., the heat lost through this process is normally neglected, leading to an over estimation of solar cell efficiencies.

1.4 COMPOUND SEMICONDUCTOR THIN FILM SOLAR CELLS

Compound semiconductor thin film solar cells are attractive option for efficient photovoltaic energy conversion. Thin film solar cells are sub-micron thick semiconductor layers, whose active material absorb sunlight and allow electrons to flow through the material to generate electricity. This process of conversion of light into electricity is called “photovoltaic effect”. The most widely used commercial solar cells are made from single crystalline Si with efficiencies reported up to 26.5% (Amonix, Inc) for commercial products [10]. A typical polycrystalline thin film has a thin (0.1 mm) layer on top known as a “window” material, which lets most of the light through the interface (hetero-junction) to the absorbing layer. The absorbing layer (1–2 mm thick) has to have a high absorption to be effective in the generation of current and a suitable band gap to provide good voltage. Considering these facts thin film solar cells can be fabricated by several techniques such as CSP and co evaporation. For this particular study, $CuInS_2/In_2S_3/Ag$ cells were fabricated by CSP technique.

1.5 FABRICATION OF $CUINS_2/IN_2S_3$/ITO CELL

For junction fabrication ITO coated glass was used as substrate. Earlier optimised spray conditions were used for fabrication of $CuInS_2$ and In_2S_3 thin film solar cells. Near stoichiometric $CuInS_2$ prepared at 300°C, 30 ml, and spray rate 1ml/min with thickness 0.30 µm. In_2S_3 layer with In/S ratio 2/8, substrate temperature 300°C, 8 ml/min was deposited over $CuInS_2$ layer. In_2S_3 layer was made thick enough so that despite the diffusion of Cu from $CuInS_2$, a layer of pure In_2S_3 remained on the top surface [12]. Silver electrodes of area 0.25 mm^2 were deposited by vacuum evaporation over In_2S_3 layer. This cell had Jsc of 4

European Journal of Business & Social Sciences
Available at https://ejbss.org/
ISSN: 2235-767X
Volume 07 Issue 01
January 2019

mA/cm^2 and V_{OC} ~ 490 mV.

1.6 PHOTOTHERMAL ANALYSIS OF $CUINS_2/IN_2S_3$ JUNCTION

1.6.1 THEORY

When a photon of energy larger than the band gap impinges upon a photovoltaic device, it is reflected, absorbed and converted into useful electricity, or absorbed and converted into heat; this can be measured using low frequency photoacoustics. This aspect has been explored by several authors for investigating photo-induced conversion processes ranging from the study of photosynthetic process in leaves to the monitoring of photovoltaic conversion efficiency of solar cells, and the study of non-radiative recombination processes in semiconductors. Apart from this, an additional heating due to internal thermal loss in the cell also contribute to photothermal signal. This was identified as due to the current dissipation at solar cell internal resistance [1]. In early PA experiments these internal losses contributions were not observed since the experiment was performed at higher modulation frequencies (> 540 Hz).

In general form, photothermal signal may be written as,

$$Signal \propto \alpha \left[\sum \left(\phi \Delta E_{p,i} / Nh\nu \right) - \left(\Phi_l \nu_l / \nu \right) - \gamma \right] \text{.....1.1}$$

Where α is the fraction of light absorbed by the illuminated sample, Φi is the quantum yield for photochemical reaction i, $\Delta E_{p,i}$ *is the molar internal change of product information in this reaction,* ν_l *and ν are frequencies of emitted and incoming radiation, N is the Avagadro number, h is the Planck's constant, γ is the energy-conversion efficiency for photovoltaic process.*

In a solar cell under photothermal analysis, if only a photovoltaic process takes place the signal can be written as,

$$Signal \propto \alpha \left[1 - \gamma (L) \right] \text{ .....1.2}$$

Where L is the specific resistance load L

Here, [*1- γ (L)*] can be termed as "photovoltaic loss" as it represents the decrease in the photothermal signal with respect to normal absorption signal, because of photovoltaic process. From equation 6.2, the photothermal conversion efficiency is given by,

$$\gamma (L) = \left[\alpha - signal(L) \right] / \alpha \text{ .....1.3}$$

By minimizing the photothermal signal (i.e., maximizing $\left[\alpha - \text{s}ignal(L) \right]$), we can find the optimum load *L* and conversion efficiency *γ* at this load. As a photovoltaic device will have zero-energy-conversion efficiency at open circuit (*OC*) condition, photothermal signal under these conditions will equal to 'α', and therefore,

$$\gamma (L) = \left[signal(OC) - signal(R_L) \right] / signal(OC) \text{ .....1.4}$$

Thus from Eq. 6.4, we can calculate the conversion efficiency of the PV device at a given R_L from ratio of the PT signal amplitude under optimal load and open circuit conditions. The importance is that we need not know the irradiance of the illuminating light and the geometry of the solar cell. According to maximum power transfer theorem, if the R_L is made larger

European Journal of Business & Social Sciences
Available at https://ejbss.org/
ISSN: 2235-767X
Volume 07 Issue 01
January 2019

than the R_S, then efficiency is higher, since a higher percentage of the source power is transferred to the load, but the *magnitude* of the load power is lower since the total circuit resistance goes up. If R_L is smaller than the R_S, then most of the power ends up being dissipated in the source, and although the total power dissipated is higher, due to a lower total resistance, it turns out that the amount dissipated in the load is reduced and γ becomes negative for $R_L << R_S$. Furthermore at matching resistance condition $R_L=R_S$ predicts γ=0. Therefore from the plot γ (R_L) of versus R_L (Figure 6.3) (as measured by Eq 6.4), we can determine R_S (using the condition when $R_L=R_S$, γ=0) and optimum R_L as the R_L where the γ is maximum.

1.6.2 EXPERIMENTAL DETAILS

The experimental set up is shown in figure 6.1. Photovoltaic device (1×1 cm^2) to be analysed is placed in the sample cell provided. In open circuit mode, the constant bias illumination is supplied by 250 W halogen lamp filtered with an IR filter. The load resistance (R_L) is connected to the solar cell device using external wires that are attached to the electrodes of the device. The material is excited with the intensity modulated pump beam (2.81 eV) using the chopper frequency of 15 Hz.

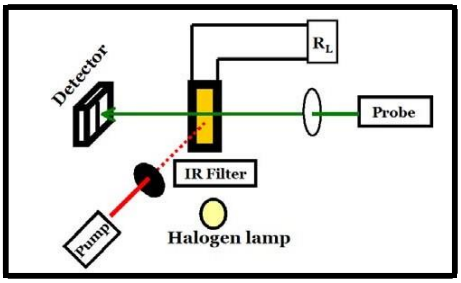

Figure 1.13 Experimental design for photothermal analysis of solar cells

1.6.3 TRANSPORT PROPERTIES

$CuInS_2/In_2S_3$ cells were irradiated with beam of energy 1.96 eV. The beam is thus absorbed entirely at the absorber layer $CuInS_2$; In_2S_3 with low absorption coefficient transmits the light to the bottom absorber layer. Figure 1.14 shows the photothermal signal variation of 'all sprayed' $CuInS_2/In_2S_3$/ITO structure. Transport properties measured from this plot gives information only on the absorber layer of the cell. The mobility was 60 mV/cm^2, lifetime (300 μs) and lowest V_{sr} (× 106 cm^2/s). We find that the mobility has considerably gone up from that of the single absorber layer and also there is decrease in the V_{sr}. Hence the deposition of In_2S_3 in the optimised composition has definitely assisted in improving the absorber layer properties..

European Journal of Business & Social Sciences
Available at https://ejbss.org/
ISSN: 2235-767X
Volume 07 Issue 01
January 2019

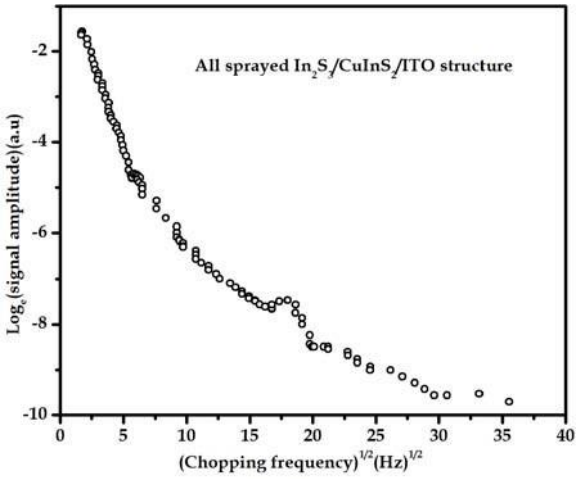

Figure 1.14 Photothermal response of $CuInS_2/In_2S_3$ solar cell

1.6.4 MEASUREMENT OF SERIES RESISTANCE, OPTIMAL LOAD RESISTANCE AND EFFICIENCY

Figure 1.16 shows variation in photovoltaic conversion efficiency as a function of load resistance. The data shown in figure 1.15 was recorded at 15 Hz and the main features may be summarized as follows; it shows an optimum load resistance at around 9 Ω, this is the value of R_L at which γ is maximum. For load resistance less than 7 Ω, γ becomes negative. It is to be noted here that R_L at 7 Ω for which γ=0 is the R_S of the cell. Conversion efficiency as calculated using this technique is ~1% which is almost same as that measured by electrical measurements (Table 1.7). Thus through photo-thermal technique we can determine the series resistance, optimum load resistance and conversion efficiency of compound semiconductor thin film solar cells.

Table 1.7:Cell parameters determined by electrical and photo-thermal measurements

Analysis	R_s (Ω)	Optimum load (Ω)	Efficiency (%)
Electric	9	–	1.15
Photothermal	7	10	1

European Journal of Business & Social Sciences
Available at https://ejbss.org/
ISSN: 2235-767X
Volume 07 Issue 01
January 2019

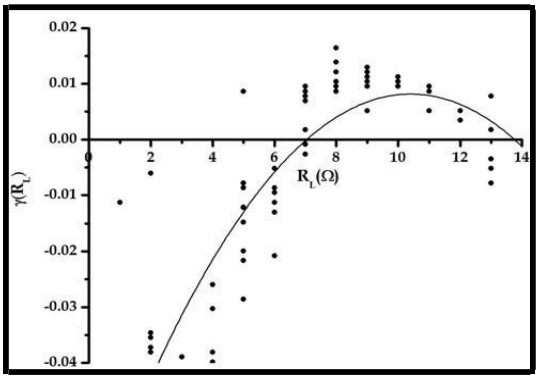

Figure 1.15 Photovoltaic conversion efficiency as function of load resistance

This application can be used for quality control of solar cell in different stages of their deposition process. In the first step the transport parameters, thermal diffusivity, μ, V_{sr} and τ_r can be determined to check quality and finally junction parameters can be determined using this technique.

1.7 CONCLUSION

The non-radiative transitions occurring in the conduction band and defect band of In_2S_3 films were analyzed using PTBD technique and the study strongly proved the role of chlorine in improving the transport properties by annihilation of non-radiative recombination centres and creation of defect bands that assist in carrier generation. The study also allowed us to find out the composition best suited for device fabrication by correlating the measured transport properties of buffer layer with the final cell parameters. Ag, which is used as electrode, when deposited over the buffer layer, improved the transport properties widely. Depth profiling, which is another important application of PTBD technique, is exploited here to study the diffusion of Ag into bulk of the material on annealing. More over the study also gave information on the period for which the Ag layer deposited on In_2S_3 remained as a separate layer. After this period, it diffused into the bulk forming a single layer.

PTBD is found to be simple and reliable tool for characterization of PV devices. This technique was applied for measuring the energy conversion efficiency, optimum load resistance and series resistance of $CuInS_2/In_2S_3$/Ag thin film solar cells. PTBD technique being a non-destructive tool and measurements are made in open circuit conditions, it can be applied to analyse partially completed solar cells, yielding information about every process in fabrication sequence. Thus PTBD is a potential tool of industrial process monitoring.

REFERENCES

- H L Riette, L C M Miranda, H Vargas 1987 Appl Phys A 44 219
- D Cahen, S Malkin, E I Lerner 1978 FEBS Letter 91 339
- C A S Lima, J C V Mattos, A F S Penna, J F W von Bulov, L C M Miranda, C C Ghizoni 1982 J Photoacoustics 1 61.

- D Cahen 1978 Appl Phys Lett 33 810
- D Cahen, S D Halle 1985 Appl Phys Lett 46 446
- C C Ghizoni, L C M Miranda 1982 Proc IEEE Ultrason Symp, New York 2 601
- G Bults, P E Nordal, S O Kanstad 1982 Biochim Biophys Acta 682 234
- I F Faria, Jr C C Ghizoni, L C M Miranda 1986 J Appl Phys 59 3294
- P Grunow, R Schieck 1995 J Appl Phys 77 2773 www.amonix.com
- P Alpuim, A Samantilleke, E Marins, F Oliveira, M F Cerqueira, L Rebouta, S Stefanov, S
- Chiussi, C Serra, J E Bourée 2010 Phys Stat Sol (c) 7 1061
- T Sebastian 2009 PhD Thesis, Cochin University of Science and Technology, India